This is a preprint version.

Published article in:
Selective thermal emission of directionally solidified Al2O3/Y3−xErxAl5O12 eutectics: Influence of the microstructure, temperature and erbium content.
P.B. Oliete, A. Orera, M.L. Sanjuán, R.I. Merino.
Solar Energy Materials and Solar Cells 174 (2018) 460–468.
Available online: 29 sept 2017. Vol 174, January 2018.
http://dx.doi.org/10.1016/j.solmat.2017.09.031

SELECTIVE THERMAL EMISSION OF DIRECTIONALLY SOLIDIFIED $Al_2O_3/Y_{3-x}Er_xAl_5O_{12}$ EUTECTICS: INFLUENCE OF THE MICROSTRUCTURE, TEMPERATURE AND ERBIUM CONTENT

P. B. Oliete*, A. Orera, M. L. Sanjuán, R. I. Merino

Instituto de Ciencia de Materiales de Aragón (ICMA), CSIC–Universidad de Zaragoza, María de Luna 3, 50018 Zaragoza, Spain.

* Corresponding author: P. B. Oliete Tel: +34 876 555 605; Fax: +34 976 761 957

E-mail addresses: poliete@unizar.es (P. B. Oliete); aorera@unizar.es (A. Orera); sanjuan@unizar.es (M. L. Sanjuán); rmerino@unizar.es (R. I. Merino)

ABSTRACT

Directionally solidified eutectic rods of Al_2O_3-$Y_{3-x}Er_xAl_5O_{12}$ ($0 \leq x \leq 3$) composition have been grown using the laser floating zone method at processing rates of 25 mm/h and 750 mm/h. For all the samples the microstructure presents the same morphology, consisting of an interpenetrated 3D eutectic network of both Al_2O_3 and garnet phases, while eutectic interspacing strongly depends on the solidification rate. Optical

absorption, luminescence and thermal emission have been investigated as a function of the growth rate and the erbium content. From the luminescence characterization it can be concluded that erbium ions are present in the eutectic only in the garnet phase. Near infrared thermal emission has been measured at temperatures ranging from 1000 to 1500ºC. Selective emission consisting of an emission band at 1540 nm and a weaker line at 970 nm, ascribed to the radiative de-excitation of the thermally excited Er^{3+} ions from the $^4I_{13/2}$ and $^4I_{11/2}$ multiplets to the $^4I_{15/2}$ ground state respectively, has been detected in all the samples containing erbium. The influence of the erbium content, the microstructure and the temperature on the thermal emission has been investigated. The strongest selective emission has been obtained for samples with x=3 although it does not increase proportionally to the erbium content. The thermal emission becomes more intense when the temperature is increased but the selective emission seems to saturate at temperatures higher than 1300º C. This effect is especially noticeable for x=3 and is attributed to thermally activated non-radiative de-excitation channels. It is suggested that these channels become effective through energy transfer among Er^{3+} ions and towards killers.

Keywords: Al_2O_3/ $Er_3Al_5O_{12}$; Directionally solidified eutectic ceramics; Selective emitters; Optical absorption; Thermophotovoltaic

1. INTRODUCTION

Erbium-based materials have been extensively studied due to their interesting optical properties that make them suitable for a wide range of applications. Different erbium doped hosts have been investigated as fibre amplifiers [1], infrared fibre lasers [2], up-conversion phosphors [3] or visible up-conversion lasers [4]. In addition, they have been proposed as selective emitters in thermophotovoltaic (TPV) devices due to their emission properties at high temperature [5].

TPV systems convert the electromagnetic radiation emitted by a material heated at high temperatures into electrical energy using photovoltaic cells [6]. The thermal emitter can be a blackbody or a grey-body, emitting in a broad spectral range, or a selective emitter, which emits in a few narrow spectral bands. The use of selective emitters with strong emissions matching the sensitive region of the photovoltaic cell increases the efficiency of the TPV device [7]. Rare-earth compounds have been investigated as selective emitters as they emit thermally in narrow bands even at high concentrations [8,9]. In particular, some erbium based materials show, when heated above 800ºC, an intense selective emission at 1.5 μm that matches with GaSb or InGaAs photovoltaic cells, making them promising candidates as selective emitters in TPV converters [10].

When choosing the material for selective emitters, the severe working conditions, with operating temperatures usually above 1000 ºC, need to be considered. Therefore, the emitter has to combine an intense selective emission with a good thermostructural performance, such as resistance to thermal shock or microstructural stability at high temperature during long periods. These requirements are a strong constraint in the selection of materials that can be used in this application. Monolithic erbium oxide

ceramics have been found to have poor thermal shock resistance, cracking when they are heated above 1000ºC [11]. The use of ceramic fibres with diameter down to 10 μm improves the thermal shock performance of the selective emitter and reduces the emission out of the rare-earth bands [12]. Recently, some directionally solidified eutectic ceramics (DSEC) incorporating Er^{3+} or Yb^{3+} ions have been investigated as selective emitters [13-15]. DSEC based on Al_2O_3 stand out for their mechanical properties and microstructural stability at temperatures close to their melting point [16-18]. The addition of rare-earth ions to the composition of DSEC allows fulfilling both the thermostructural and the functional requirements for selective emitters.

Numerous studies have been addressed to enhance the intensity of the selective emission of erbium-based materials. The influence of the host material in the thermal emission has been previously reported [10,19]. The performance of the selective emitter upon variation of the rare earth ion content has also been investigated. In principle, when increasing the Er^{3+} concentration the selective emission should be more intense, as more Er^{3+} ions can be found in the excited state and from that, more radiative de-excitation is expected. However, some works on the selective emission in Er:YAG [19] and in Yb:YAG and Yb:Y_2O_3 [20] show that the specific emission decreases with the increase of the rare-earth ion content. Upon rising the temperature, the selective emission is also expected to increase. Nevertheless, a recent study of the thermal emission of Yb^{3+} ions in DSEC reports that although the thermal emission increases with the temperature as expected, a saturation of the selective emission at temperatures above 1300º C is observed [15].

The 4f excited levels of the rare earth ion that give rise to the selective thermal emission become populated, for low density of the electromagnetic radiation, through the interaction of the electronic system of the rare earth ions with the phonon thermal

bath, as explained by Golovlev [21]. Consequently, electron-phonon interaction is a requisite for the efficient population of the upper levels. On the other side, it also generates non-radiative de-excitation by multiphonon emission. This causes, for example, thermal quenching of the luminescence [22]. Moreover, it has already been documented that in concentrated systems, electron-phonon interactions are enhanced, causing for example intense vibronic transitions [23] or increased multiphonon relaxation processes due to the contribution of phonon assisted energy transfer [24,25]. Therefore, a change in the concentration of the active rare earth ion not only modifies the amount of ions contributing to the selective thermal emission, but also the quantum interactions that promote it.

In this work, directionally solidified Al_2O_3-$Y_{3-x}Er_xAl_5O_{12}$ ($0 \leq x \leq 3$) eutectic rods have been fabricated using the laser floating zone (LFZ) technique. The large thermal gradients at the liquid/solid interface achieved with this technique have allowed the use of high growth rates. Varying the growth parameters, samples with different microstructures have been obtained. The optical properties (absorption and luminescence) have been measured at room temperature. The thermal emission has been studied up to 1500ºC as a function of the erbium content and microstructure. The aim of this work is to investigate the relationship between the erbium selective emission and both the composition and microstructure of the eutectics, and to understand its dependence on the temperature in order to optimize the performance of the material as a selective emitter.

2. MATERIALS AND METHODS

Eutectic rods of Al_2O_3-$Y_{3-x}Er_xAl_5O_{12}$ ($0 \leq x \leq 3$) were directionally solidified using the LFZ method. Ceramic powders were prepared using a mixture of commercial powders of Er_2O_3 (Alfa Aesar, 99.99%), Al_2O_3 (Aldrich, 99.99%) and Y_2O_3 (Aldrich 99.99%) with the eutectic compositions given in Table 1. Cylindrical precursors were fabricated by isostatically pressing the powder for 3 min at 200 MPa and sintering at 1500 ºC during 4 hours.

Eutectic rods were processed using a CO_2 laser as heating source. The growth was performed in a nitrogen atmosphere, with a slight overpressure of 0.1-0.25 bar with respect to ambient pressure to avoid the appearance of gas inclusions in the solidified rod [26]. Two processing rates (25 and 750 mm/h) were used to obtain eutectics with different microstructures. The solidified rods presented a final diameter varying between 1.3 and 1.6 mm. A reduction of the rod diameter was achieved when necessary by setting a lower speed to the precursor than to the grown rod. From now on, the different Al_2O_3-$Y_{3-x}Er_xAl_5O_{12}$ processed ceramics will be referred to using the acronym AEx. $Er_3Al_5O_{12}$ (EAG) single crystals were also grown in air using the same procedure and a growth rate of 50 mm/h, with the precursor composition given in Table 1.

Transverse and longitudinal cross-sections of the eutectic rods were cut and polished for scanning electron microscopy analysis. The microstructure was studied using the back-scattered electron images obtained in a Field Emission SEM (model Carl Zeiss MERLIN).

The optical absorption spectra were measured on a Cary 5000 UV-VIS-NIR spectrophotometer from Agilent. For that purpose, thin slices of around 150 μm were cut transverse to the growth direction and polished.

RT Luminescence in the 540-570 nm region was excited either with the 514.5 nm line of an Ar^+ laser through a microscope (50X objective lens) and 10 mW of incident power, or with a 1000 W tungsten lamp passed through a 0.5 m monochromator centred at 488 nm and band-pass of 10.8 nm. The luminescence was focussed on the entrance slit of a monochromator and then detected with a multichannel CCD detector or sequentially with a Hamamatsu 980 photomultiplier tube respectively.

Thermal emission spectra were measured on the as-grown rods inside the growth chamber by heating the samples with a CO_2-laser focused annularly on the sample surface, producing a heated surface ≈1 mm high. The emitted light was collected using a 1000 μm diameter optical fibre yielding an acceptance angle of 25.4º. The fibre was reproducibly positioned at ≈30 mm from the sample. The emission was detected in the 1000-2500 nm range using a NIR 256-2.5 spectrophotometer from Ocean Optics. The spectral sensitivity of the spectrometer was calibrated using a halogen lamp with the brightness temperature of 2968 K. Temperature was varied from 1000ºC to 1500ºC by changing the laser power and measured using a two-colour pyrometer (Impac, ISR12-LO MB33).

3. RESULTS AND DISCUSSION

3.1. Microstructure

Scanning electron micrographs showing the microstructure of the transverse cross-section of the eutectic samples grown at 25 and 750 mm/h with different erbium contents are presented in Fig. 1. All the samples were found to be free of voids and cracks and presented a homogeneous microstructure throughout the entire cross-section of the grown rod. In all cases the microstructure consisted of a three-dimensional

interpenetrating network of Al_2O_3 (dark contrast) and garnet (light contrast) domains, and no other phases were detected in the scanning electron microscope. Similar microstructures have been previously reported in different directionally solidified Al_2O_3-garnet eutectics [16-18]. The tendency of the component phases to develop facets was evident at low growth rates, as a result of their high entropy of melting (48 J/K·mol for Al_2O_3 and 122 J/K·mol for $Y_3Al_5O_{12}$, which is expected to be very close to that of $Er_3Al_5O_{12}$) [27].

The volume fractions of the Al_2O_3 phase were estimated from the SEM micrographs and presented in Table 1. No significant differences were observed upon varying the growth rate or the erbium content, and the experimental values were roughly close to the volume fractions calculated from the eutectic composition (45% for AE0, 44% for AE3).

The microstructural size was strongly dependent on the growth rate, the size of the phases decreasing as the growth rate increased, according to the Hunt-Jackson law [28], $\lambda^2 \cdot v = C$, where λ is the eutectic interspacing, v the growth rate, and C a constant depending essentially on the phase diagram and the diffusion coefficient of the ions in the melt. The eutectic interspacing was measured using linear interception methods and decreased from 5-6 μm in samples grown at 25 mm/h down to 1 μm in those solidified at 750 mm/h (see Table 1).

3.2. Optical absorption

VIS-IR room temperature in-line transmission spectra of AE3 samples grown at different rates were reported by M.C. Mesa et al [14]. They consist of a scattering associated background on top of which absorption bands were observed, corresponding

to transitions from the $^4I_{15/2}$ to the excited multiplets of the $4f^{11}$ configuration of Er^{3+} in the garnet phase. As scattering affects not only the background but also the apparent intensity of the Er^{3+} absorption bands [14], and scattering is smaller the smaller the microstructure, we show in figure 2 the in-line NIR transmission spectra of samples solidified at 750 mm/h for the three compositions, x = 3, 0.3 and 0.03. The spectra were taken on slices around 140 to 150 μm thick, so that comparison of background and absorption band intensities is meaningful. The plotted extinction or attenuation coefficient has been calculated from the measured in-line optical density, *OD*, and sample thickness, *d*, as $(2.303/d)\cdot OD$. Note that the attenuation coefficient includes losses due to both absorption and scattering processes.

As expected, the scattering background increases towards short wavelengths, in a similar way for the three samples. The absorption bands around 1500 nm and 950 nm correspond to transitions from the $^4I_{15/2}$ ground multiplet to the $^4I_{13/2}$ and $^4I_{11/2}$ multiplets of Er^{3+} respectively. Their intensities increase as the erbium content increases, although they are not fully proportional. If we take the erbium concentration values given in Table 1, we can estimate a phenomenological oscillator strength for the $^4I_{15/2}$ to $^4I_{13/2}$ transition (see Ref. [14] for details) that takes values of 2.2×10^{-6} for AE3 and 2.6×10^{-6} for AE03. The estimate of the oscillator strength for the diluted sample has large uncertainties coming from the background subtraction procedure. Alternatively, comparing the erbium band intensity at peak wavelength, it can be seen that that of AE03 is 10 times larger than that for AE003, while in the case of AE3 it is only around 8.5 times that of AE03, being the erbium concentration 10 times larger. As the microstructure size and shape (and expected scattering) are almost the same irrespective of the erbium content (see Table 1), we must conclude that, in these eutectic materials, the oscillator strength of EAG is 15% smaller than that of YAG:0.1 Er or YAG:0.01 Er.

3.3. Luminescence

With the aim of verifying whether additional Er^{3+} sites are created (for instance, in the Al_2O_3 part of the eutectic bi-crystal) or the occurrence of any modification in the environment around the usual rare-earth site in YAG, the emission of the AEx samples from the $^4S_{3/2}$ to the $^4I_{15/2}$ multiplet around 550 nm was measured at room temperature. Two different excitation sources were used: an Ar^+ laser at 514.5 nm, exciting into the $^2H_{11/2}$ multiplet, and a lamp + monochromator with 10.8 nm band pass centred at 488 nm, which reaches the $^4F_{7/2}$ multiplet.

The $^4S_{3/2}$ to $^4I_{15/2}$ luminescence spectra of Er^{3+} in AE003, AE03 and AE3 eutectic rods grown at 25 mm/h and in the garnet single crystal EAG are presented in figure 3. For comparison, we include in the figure the luminescence spectrum of the AE03 sample excited with the lamp at 488 nm. The lower resolution of the latter spectrum is due to the larger slit used in this experiment, compared with that of the laser-excited spectra. Small energy shifts are observed in the eutectic samples as a function of the erbium content, which can be attributed to slight differences on the lattice parameters and local environment of the Er^{3+} ions. On the other hand, remarkable intensity differences are observed, not fulfilling the proportionality to erbium content, which is ascribed to concentration quenching of the luminescence. Except for these two factors, the spectra are fully in agreement with the luminescence of Er^{3+} ions in the YAG host or in EAG [29-31], which implies that there are no additional sites besides those of the garnet structure, in particular that there is no erbium in the Al_2O_3 phase. No differences were found between samples solidified at 25 or 750 mm/h. The emission spectra under laser or wide-band excitation are also remarkably coincident. The similarity of the

spectra excited with a laser or a wide band lamp suggests that no selective excitation of a specific Er^{3+} site is taking place when using the laser source.

The origin of each band has been identified according to the expected splitting of the $^4S_{3/2}$ and $^4I_{15/2}$ multiplets of an Er^{3+} ion in a crystal field of D_2 symmetry (Wyckoff site 24c of the Ia-3d garnet structure) into 2 and 8 Kramers doublets, respectively, as shown in figure 4. The vertical sticks in figure 3 show the assignment of the bands according to the initial and final states of the electronic transition. Both sets differ by ~ 65 cm^{-1}, which is the splitting of the $^4S_{3/2}$ multiplet, and denote the transitions to the eight doublets of the ground $^4I_{15/2}$ multiplet.

The splittings of the $^4S_{3/2}$ and $^4I_{15/2}$ multiplets for AE003, AE03 and AE3 samples are given in figure 4. The level scheme is in agreement with that reported in the literature for Er^{3+} in YAG or EAG [29-31], implying that the rare earth environment in eutectic systems is similar to that of bulk single crystals or polycrystalline materials.

3.4. Thermal emission

Emission at temperatures between 1000 and 1500ºC was measured in the near infrared spectral region for all the samples. Figure 5 shows the thermal emission of AE0, AE003, AE03 and AE3 eutectic rods grown at 750 mm/h at 1200 ºC. Only samples containing erbium showed selective emission. The emission spectra in samples containing erbium consist of an intense relatively narrow band centred in 1540 nm and a weak band at 970 nm with an off-band emission almost negligible at this temperature in the measured wavelength range. Emission was ascribed to the radiative de-excitation of the thermally excited Er^{3+} ions from the $^4I_{11/2}$ and $^4I_{13/2}$ states to the $^4I_{15/2}$ ground state.

Influence of the erbium content

As shown in figure 5, the selective emission bands become more intense when the erbium content increases. However, the intensity does not correlate proportionally with the erbium concentration, neither with the Er^{3+} absorption given in figure 2. This was also pointed out by D. L. Chubb et al [9], whose calculations for a non-scattering medium demonstrated that for large values of the optical depth, the emissivity is independent of the absorption coefficient. Figure 6 shows the integrated area of the selective emission bands (background subtracted) measured at 1200ºC as a function of the erbium content for AE003, AE03 and AE3 rods solidified at 750 mm/h. As a guide, solid lines show the linear dependence of the emission with the erbium content. We can observe that the integrated intensities corresponding to the $^4I_{11/2} \rightarrow {}^4I_{15/2}$ transition (970 nm) approximately scale with the erbium content. On the contrary, the emission ascribed to the $^4I_{13/2} \rightarrow {}^4I_{15/2}$ electronic transition (1540 nm) is clearly truncated in samples with x=3.

The slower than proportional increase of the 1540 nm band intensity as a function of the erbium content is accompanied by changes in the band shape and half-width. The inset in figure 5 presents the emission band centred at 1540 nm normalized to the maximum amplitude for all the samples. We can notice that when the erbium concentration increases, the selective emission band broadens. In addition, the structure due to the Stark components of the electronic levels is more clearly resolved in the diluted samples.

The broadening of the thermal emission bands (resolution loss) and concomitant increase of emissivity at a lower rate than the erbium concentration is easily understood if one considers self-absorption of the emitted light before leaving the sample. The

emissivity in these dense materials is a volume property, and thus increases as the size (thickness) of the emitter increases. A very rough estimate of the dependence of selective emissivity versus sample thickness can be done assuming that the material is non-scattering and semitransparent. Under such conditions, from Kirchhoff law the emissivity can be calculated from the absorptivity using equation 17.3 from reference [32]:

$$\varepsilon = (1 - R)\frac{1-exp(-\alpha d)}{1-R\ exp(-\alpha d)} \qquad (1)$$

where R is the one-surface reflectance, d is the sample thickness and α is the absorption coefficient (just the Er^{3+} contribution to extinction in our case).

Eq. (1) immediately shows that emissivity keeps proportionality to absorption coefficient only if the optical thickness (αd) is $\alpha d << 1$. In fact, for $\alpha d = 4$ it practically saturates to its maximum value, (1-R). α-values for AE3 at room temperature can be obtained from figure 2, subtracting the background, and the same spectrum can be used scaled down by 1/8.5 and 1/85 to account for absorption in AE03 and AE003 respectively. In figure 7 we have used thickness d = 1 mm, as it is an appropriate value to compare with our experimental thermal emission bands. R can be estimated assuming n = 1.8 for the eutectic ceramic. Figure 7 roughly reproduces the concentration dependence of emission observed in figure 5. The peaks at 1457 nm, 1470 nm and 1531 nm in AE3, with peak absorption coefficients above 40 cm^{-1} and $\alpha d > 4$, are clearly truncated, which causes broadening of the emissivity band. Besides, the different dependence on the erbium content of the emission corresponding to the $^4I_{11/2} \rightarrow {}^4I_{15/2}$ and $^4I_{13/2} \rightarrow {}^4I_{15/2}$ electronic transitions can be explained with this model. The absorption

coefficient of the band centred at 970 nm is four times lower than that of the band at 1531 nm, which greatly reduces the truncation of the emissivity at this wavelength. This same effect would result from an increase in the sample thickness, as long as a non-scattering material can be assumed. When scattering plays a role, both contributions are not completely equivalent, but the tendencies are the same as long as scattering is not very strong.

In order to prove experimentally the influence of the thickness in the thermal emission, an AE3 eutectic rod of 0.3 mm in diameter was fabricated by LFZ using several diameter reduction stages and a final growth rate of 25 mm/h. Figure 8 shows the thermal emission of this rod at 1200º C compared with that of an AE3 eutectic rod of 1.4 mm in diameter grown at the same processing rate. For comparison purposes, both spectra were normalized to their maximum intensity. We can observe that the diameter reduction results in a narrower spectrum, with more resolved Stark structure and a less intense component at 1608-1630 nm. All these features are in agreement with a smaller truncation, as predicted by the calculations.

Influence of the temperature and microstructure

The selective emission of the eutectic rods AE003, AE03 and AE3 was studied as a function of temperature and microstructure. Figure 9 shows the thermal emission spectra of the AE03 and AE3 rods grown at 25 mm/h and 750 mm/h at different temperatures. No significant differences were found between the samples grown at 25 mm/h and 750 mm/h, indicating the small influence of the microstructure size in the thermal emission. The selective emission increased when the temperature rose as a consequence of the higher thermal excitation of erbium ions. The position and half-width of the lines remained essentially the same with increasing temperature. The off-

band emission in the measured range, almost negligible at 1000ºC, also became more intense when the temperature was increased.

The rates at which selective and off-band emissions raised with temperature were very different for AE3 samples compared to those of the other compositions. Figure 10 shows the integrated intensity (background subtracted) of the selective emission bands around 970 nm and 1540 nm for AE3, AE03 and AE003 and the intensity value for AE3 out of the Er^{3+} bands (1200 nm and 1900 nm) as a function of the temperature. These emission intensities are compared with the blackbody radiation at the corresponding wavelengths. We can observe that out of the erbium emission band (1200 nm, figure inset), the thermal emission of AE3 increases with temperature as predicted by Planck´s law. At 1900 nm it seems to increase with temperature even faster. However, at the wavelengths corresponding to the maxima of the Er^{3+} bands, the selective emission increases with temperature less than expected. This is particularly remarkable in sample AE3, where only slight variations of the selective emission could be detected at temperatures higher than 1300ºC. The selective emission of the AE03 and AE003 samples presents a significantly lower thermal saturation than that measured in the AE3 rods. No significant variations of the tendency to thermal saturation were observed with the microstructure of the samples. The thermal saturation of the selective emission has been recently reported for Al_2O_3-$Yb_3Al_5O_{12}$ eutectic ceramics [15] and was attributed to the competition between the increase of the thermal population of the excited state with the temperature and the enhancement of the multi-phonon non-radiative de-excitation.

As pointed out in the introduction, the electron-phonon interaction is responsible both for non-radiative multiphonon excitation and de-excitation processes, which are more active for concentrated systems than for diluted ones. De-excitation takes place by

the emission of a number of phonons required to span the appropriate energy gap to a lower electronic level, while the excitation requires the absorption of phonons. Both are enhanced as the electron-phonon interaction increases and also with temperature. If they are large enough to be the dominant processes in populating the rare earth ion excited states, they keep the thermal equilibrium population and emissivity should follow the temperature dependence predicted by Planck´s law.

The experimental results presented in figure 10 indicate however that at least for the more concentrated samples AE3 and AE03 there must be an extra contribution to de-excitation that diminishes the population of the emitting level below that corresponding to the thermal equilibrium, and that this contribution is more effective at high temperatures. Such depopulation can be produced in rare-earth ion luminescent materials by energy transfer and de-excitation to sparsely distributed killers [33]. Therefore, to explain the saturation of the thermal emission at high temperature we propose as a plausible mechanism a thermally activated energy transfer to killers. Note that in erbium doped YAG concentration quenching already exists [34], and explains, for example, the decrease of the green luminescence with increasing the erbium content presented in figure 3.

Such de-excitation at the killer centres will be in general thermally activated, as observed in lower temperature spectroscopic studies [35]. Unknown centres will act as acceptors of the transfer process, followed most probably by non-radiative de-excitation but with small probability of back-transfer towards the electronic Er^{3+} subsystem, thereby decreasing the population in the excited states and their associated thermal emission. The larger the concentration, the faster the energy transfer among Er^{3+} ions and eventually to the killers. Because of its fast thermal activation, the energy transfer process is able to overcome competing re-equilibration processes, namely multiphonon

excitation and de-excitation events, and results in the observed slowing down of the thermal emission with increasing temperature. The overall effect of this proposed energy transfer to killers would be the depopulation of specific excited state levels of the Er^{3+} subsystem. Then, electron-phonon and radiative interactions equilibrate the excited Er^{3+} level population to a smaller temperature for the electronic subsystem.

Analysis of the saturation of the selective thermal emission with temperature.

In an attempt to explain the temperature dependence of the Er^{3+} emission within the proposed model for the different AEx samples, we have written the rate equations for the electronic populations of the ground, first and second excited Er^{3+} multiplets, i.e. $^4I_{15/2}$ (level 1), $^4I_{13/2}$ (level 2) and $^4I_{11/2}$ (level 3). For convenience we have used the same notation as in ref. [21]. In a first approach (absence of energy transfer to killers), the equations for the number of excited ions in levels 2 and 3 per unit volume are written as

$$dN_2/dt = \theta_{12}N_1 + (\theta_{32} + \gamma_{32} + \Gamma_{32})N_3 - (\gamma_{21} + \theta_{23} + \theta_{21} + \Gamma_{21})N_2 \qquad (2)$$

$$dN_3/dt = \theta_{13}N_1 + \theta_{23}N_2 - (\gamma_{31} + \gamma_{32} + \theta_{31} + \Gamma_{31} + \theta_{32} + \Gamma_{32})N_3 \qquad (3)$$

where γ_{ij} are the spontaneous radiative rates and θ_{ij} and Γ_{ij} are the induced and spontaneous non-radiative (nr) rates, respectively. The equation for N_1 is unnecessary since it is derived from the above ones through $N_1+N_2+N_3= N$, N being the concentration of Er^{3+} ions. Following [21], we have assumed that our system is radiating to a cold photon bath and thus induced radiative transitions have been neglected. This is a good approximation at the temperatures of interest here for the samples with x = 0.3 and x=3, in which the non-radiative transitions dominate over the radiative ones. For x=0.03 and T< 1100 ºC this approximation starts to fail, and deviations are observed.

The above expressions reflect the fact that the $^4I_{13/2}$ multiplet is populated by induced nr transitions from the ground state and from the nr decay (spontaneous and induced) from the $^4I_{11/2}$ multiplet, as well as by the radiative decay from the $^4I_{11/2}$ level, whereas it is depopulated trough radiative and nr transitions to the ground state and also through induced nr transitions to the third multiplet. Similarly, the $^4I_{11/2}$ multiplet is populated through induced nr transitions from the ground state and from the $^4I_{13/2}$ multiplet, whereas it is depopulated by radiative and nr decays to the ground and first excited multiplets.

In the stationary situation all populations are constant with time, which yields

$$N_2/N_1 = [\theta_{12} + (\theta_{32} + \gamma_{32} + \Gamma_{32})\, N_3 / N_1] / [\, \gamma_{21} + \theta_{23} + \theta_{21} + \Gamma_{21}] \qquad (4)$$

$$N_3/N_1 = [\theta_{13} + \theta_{23} N_2 / N_1] / [\, \gamma_{31} + \gamma_{32} + \theta_{31} + \Gamma_{31} + \theta_{32} + \Gamma_{32}]. \qquad (5)$$

Emission rates per unit volume are given by

$$I\,(^4I_{13/2}) = N_2\, \gamma_{21} \text{ for the band at 1540 nm, and} \qquad (6)$$

$$I\,(^4I_{11/2}) = N_3\, \gamma_{31} \text{ for the band at 970 nm.} \qquad (7)$$

Expressions for N_i/N can be derived through the relation $N_1+N_2+N_3= N$ but since even at the highest temperature achieved in our experiments $E_2, E_3 >> kT$ the condition $N_2, N_3 << N_1$ is fulfilled so that the error introduced by using N_1 instead of N is small.

We now assume that nr processes consist of multiphonon transitions involving creation or absorption of phonons of the appropriate energy $\hbar\omega$ and number p matching the energy difference E_{ij} between the initial and final states, i.e. $E_{ij} = p \cdot \hbar\omega$,

$$\theta_{ij} = W^0_{ij}\, n^p, \text{ and} \qquad (8)$$

$$\theta_{ij} + \Gamma_{ij} = W^0_{ij}\, (n+1)^p, \qquad (9)$$

where n is the Bose population factor for phonons of energy $\hbar\omega$, $n = (\exp(\hbar\omega/kT) - 1)^{-1}$, k is the Boltzmann constant and the nr prefactor W^0_{ij} is the nr rate at T=0 K. The radiative rates γ_{ij} are assumed to be temperature independent.

Within these assumptions the populations of the $^4I_{13/2}$ and $^4I_{11/2}$ multiplets increase monotonically with temperature in a Boltzmann-like manner, as expected by considering the ensemble of Er^{3+} ions to be in thermal equilibrium. To explain the saturating behaviour observed at high temperature, we introduce an extra de-excitation term accounting for the phonon assisted energy transfer to killers, without back transfer. Just for modelling purposes, this term is given a multiphonon dependence of the form $W_{ET}\, n^p$. The temperature dependence of the $^4I_{13/2}$ and $^4I_{11/2}$ emission bands has been simulated within this extended model to fit to the experimental data. Some constraints are imposed to limit the number of parameters. For instance, the same phonon is assumed to be involved in the multiphonon transitions between levels, and the population of the ground multiplet is assumed to be very close to N. The values of the spontaneous radiative transition probabilities have been taken from the literature as $\gamma_{21} = 143\ s^{-1}$ [36], $\gamma_{31} = 110\ s^{-1}$ and $\gamma_{32} = 26\ s^{-1}$ [37]. Energy gap law expressions and parameters for other oxides from the literature have been used as starting values for the multiphonon transition probabilities, W^0_{ij}. In particular we have used $W^0_{ij} = A \exp(-\alpha(\Delta E - 2\hbar\omega))$ to estimate multiphonon transitions in the diluted samples, with $\alpha = 0.0049$ cm, $A = 3.2 \cdot 10^7\ s^{-1}$, appropriate for $YAlO_3$ [22] and $W^0_{ij} = B \exp(-\beta(\Delta E))$ for the x=0.3 and x=3 samples, with $\beta = 0.0025$ cm [38] and $B = 10^8\ s^{-1}$. A group of parameters that reproduce the experimental dependence is given in Table 2. Solid lines in figure 10 correspond to the emission intensities calculated using the parameters in Table 2 and the expressions given in the text. Note that this fitting is the result of trial and error calculations with reasonable parameters chosen in a limited range of variation. In order

to explain the thermal saturation, the energy transfer to killers term needs to grow with temperature faster than the other contributions. Therefore, 16 phonons of energy 180 cm^{-1} are involved in the energy transfer process. These phonons are of a much lower energy than those associated to the other non-radiative processes (around 500 cm^{-1}). As expected, the probability of transfer to killers (W_{ET} coefficient in table 2) increases with the erbium content, since energy migration is faster and the probability to find a killer is higher.

In conclusion, energy transfer to killers without back transfer can deplete thermal emission at high temperatures in rare earth containing dielectrics, limiting the optimal maximum operating temperature. In these highly doped selective emitters, the use of temperatures above 1300ºC does not produce a significant increase of the erbium thermal emission, whereas the off-band intensity rises as that of the black body, which results in a loss of selectivity.

It is worth noting that, despite the larger depletion of the selective thermal emission at high temperatures for concentrated samples and the emission truncation associated to erbium self-absorption processes, the thermal radiation emitted by the AE3 eutectic rod in the spectral range matching the active region of the GaSb or InGaAs photovoltaic cells is at every temperature quite more intense than in diluted samples. Therefore, the use of AE3 selective emitters in TPV converters will produce higher emitted power than those based in erbium diluted samples.

4. Conclusions

Selective emitters based on Al_2O_3-$Y_{3-x}Er_xAl_5O_{12}$ ($0 \leq x \leq 3$) eutectic ceramics were fabricated by directional solidification using the LFZ method at two different growth

rates. For all the compositions the microstructure consisted of an interpenetrated network of both eutectic phases with the size of the phases strongly depending of the solidification rate, following the Hunt-Jackson law.

The optical properties at room temperature and the thermal emission up to 1500ºC were investigated for all the compositions and growth rates. An intense emission band at 1540 nm and a weaker one at 970 nm were measured in all the samples containing erbium and ascribed to the radiative decay of the thermally excited Er^{3+} ions. The matching of the stronger emission at 1540 nm with the sensitive region of some photovoltaic cells makes these eutectics suitable as selective emitters for TPV converters.

Selective emission increased with the erbium content, although it did not scale with x as a consequence of self-absorption processes of the light emitted, which produced a truncation of the emissivity in samples with high optical thickness. A concentration dependent saturation of the selective emission when the temperature increases was observed. A simple model including thermally activated energy transfer to killers allowed explaining the thermal saturation as the erbium content increases. At low erbium concentration, the non-radiative decay is mainly through multiphonon de-excitation, which is compensated by multiphonon stimulated population of the excited levels, whereas at x= 0.3 and 3 energy transfer mechanisms become increasingly dominant.

Acknowledgements

The authors gratefully acknowledge the financial support from the Ministerio de Economía y Competitividad de España under projects MAT2013-41045-R and

MAT2016-77769-R. Authors also acknowledge the use of Servicio de Microscopia Electrónica (Servicios de Apoyo a la Investigación), Universidad de Zaragoza. The authors also wish to thank Dr. Víctor M. Orera and Dr. Rafael Cases for fruitful discussions.

References

[1] K. Kuroda, Y. Yoshikuni, Wavelength-resolved measurement of gain recovery in an erbium-doped fiber amplifier, Microw. Opt. Technol. Lett. 58 (2016) 751-754.

[2] S.D. Jackson, Towards high-power mid-infrared emission from a fibre laser, Nature Photon. 6 (2012) 423-431.

[3] H.L. Xu, S. Kröll, Upconversion dynamics in Er^{3+}-doped YAG, J. Lumin. 111 (2005) 191-198.

[4] H. Scheife, G. Huber, E. Heumann, S. Bar, E. Osiac, Advances in up-conversion lasers based on Er^{3+} and Pr^{3+}, Opt. Mater. 26 (2004) 365-374.

[5] B. Bitnar, W. Durisch, J. C. Mayor, H. Sigg, H.R. Tschudi, Characterisation of rare earth selective emitters for thermophotovoltaic applications, Sol. Energy Mater. Sol. Cells 73 (2002) 221-234.

[6] T. J. Coutts, An overview of thermophotovoltaic generation of electricity, Sol. Energy Mater. Sol. Cells 66 (2001) 443-452.

[7] A. Licciulli, D. Diso, G. Torsello, S. Tundo, A. Maffezzoli, M. Lomascolo, M. Mazzer, The challenge of high-performance selective emitters for thermophotovoltaic applications, Semicond. Sci. Technol. 18 (2003) S174–S183.

[8] G.E. Guazzoni, High-Temperature Spectral Emittance of Oxides of Erbium, Samarium, Neodymium and Ytterbium, Appl. Spectr. 26 (1972) 60–65.

[9] D.L. Chubb, A.M.T. Pal, M.O. Patton, P.P. Jenkins, Rare Earth Doped High Temperature Ceramic Selective Emitters, J. Eur. Ceram. Soc. 19 (1999) 2551-2562.

[10] D. Diso, A. Licciulli, A. Bianco, M. Lomascolo, G. Leo, M. Mazzer, S. Tundo, G. Torsello, A. Maffezzoli, Erbium containing ceramic emitters for thermophotovoltaic energy conversion, Materials Science and Engineering B98 (2003) 144-149

[11] G.E. Guazzoni, E. Kittl, Cylindrical erbium oxide radiator structures for thermophotovoltaic generators, R & D Tech. Rep. ECOIM-4249. U. S. Army Electronics Command, Fort Monmouth, New Jersey (1974).

[12] R.E. Nelson, Rare earth oxide TPV emitters, In Proceedings of the 32nd International Power Sources Symposium. Electrochemical Society, Pennington, NJ, 1986, pp. 95-100.

[13] N. Nakagawa, H. Ohtsubo, Y. Waku, H. Yugami, Thermal emission properties of $Al_2O_3/Er_3Al_5O_{12}$ eutectic ceramics, J. Eur. Ceram. Soc. 25 (2005) 1285–1291.

[14] M.C. Mesa, P.B. Oliete, R.I. Merino, V.M. Orera, Optical absorption and selective thermal emission in directionally solidified Al_2O_3-$Er_3Al_5O_{12}$ and Al_2O_3-$Er_3Al_5O_{12}$-ZrO_2 eutectics, J. Eur. Ceram. 33 (2013) 2587–2596.

[15] P.B. Oliete, M.C. Mesa, R.I. Merino, V.M. Orera, Directionally solidified Al_2O_3-$Yb_3Al_5O_{12}$ eutectics for selective emitters, Sol. Energy Mater. Sol. Cells 144 (2016) 405–410.

[16] Y. Waku, N. Nakagawa, T. Wakamoto, H. Ohtsubo, K. Shimizu, Y. Kohtoku, High-temperature strength and thermal stability of a unidirectionally solidified Al_2O_3/YAG eutectic composite, J. Mater. Sci. 33 (1998) 1217–1225.

[17] J.Y. Pastor, J. LLorca, A. Salazar, P.B. Oliete, I. de Francisco, J.I. Peña, Mechanical Properties of Melt-Grown Alumina–Yttrium Aluminum Garnet Eutectics up to 1900 K, J. Am. Ceram. Soc. 88 (2005) 1488–1495.

[18] M.C. Mesa, P.B. Oliete, A. Larrea, Microstructural stability at elevated temperatures of directionally solidified $Al_2O_3/Er_3Al_5O_{12}$ eutectic ceramics, J. Crys. Growth 360 (2012) 119-122.

[19] D. Diso, A. Licciulli, A. Bianco, G. Leo, G. Torsello, S. Tundo, A. De Risi, M. Mazzer, Selective emitters for high efficiency TPV conversion: materials preparation and characterisation, AIP Conf. Proc. 653 (2003) 132-141.

[20] J.C. Panitz, M. Shubnell, W. Durisch, F. Geiger, Influence of ytterbium concentration on the emissive properties of Yb:YAG and Yb: Y_2O_3, AIP Conf. Proc. 401 (1997) 265-276.

[21] V.V. Golovlev, C.H. Winston Chen, W.R. Garrett, Heat to light energy conversion by emitters doped with rare-earth metal ions, Appl. Phys. Lett. 69 (1996) 280-282.

[22] B. Henderson, G.F. Imbush, Optical Spectroscopy of Inorganic Solids, Clarendon Press, Oxford, 1989.

[23] V.M. Orera, L.E. Trinkler, R.I. Merino, A. Larrea, The optical properties of the Nd^{3+} ions in $NaGaO_3$ and $LaGaO_3$:Nd: temperature and concentration dependence, J. Phys.: Condens. Matter. 7 (1995) 9657-9673.

[24] F. Auzel, A fundamental self-generated quenching center for lanthanide-doped high-purity solids, J. Lumin. 100 (2002) 125-130.

[25] T. Miyakawa, D.L. Dexter, Phonon sidebands, multiphonon relaxation of excited states and phonon-assisted energy transfer between ions in solids, Phys. Rev. B 1 (1970) 2961-2969

[26] P.B. Oliete, J.I. Peña, Study of the gas inclusions in $Al_2O_3/Y_3Al_5O_{12}$ and $Al_2O_3/Y_3Al_5O_{12}/ZrO_2$ eutectic fibers grown by laser floating zone, J. Cryst. Growth 304 (2007) 514-519.

[27] J. LLorca , V.M. Orera, Directionally-solidified eutectic ceramic oxides, Prog. Mat. Sci. 51 (2006) 711-809.

[28] K.A. Jackson, J.D. Hunt, Lamellar and Rod Eutectic Growth, Trans. Metal. Soc. AIME 236 (1966) 1129–1142.

[29] J.A. Koningstein, J.E. Geusic, Energy levels and crystal-field calculations of Er^{3+} in yttrium aluminum garnet, Phys. Rev. A 136 (1964) 726-728.

[30] E. Orlich, S. Hüfner, P. Grünberg, Crystal field interaction in erbium garnets, Z. Phys. 231 (1970) 144-153.

[31] J.B. Gruber, A. Nijjar, D.K. Sardar, R.M. Yow, C.C. Russell III, T.H. Allik, B, Zandi, Spectral analysis and energy-level structure of Er^{3+} ($^4f^{11}$) in polycrystalline ceramic garnet $Y_3Al_5O_{12}$, J. Appl. Phys. 97 (2005) 063519.

[32] J.R. Howell, R. Siegeland, M.P. Mengüç, Thermal Radiation Heat Transfer, 5th Ed., CRC Press. Taylor & Francis Group, LLC., Boca Raton, Florida, 2010.

[33] D.L. Huber, Fluorescence in the presence of traps, Phys. Rev. B 20 (1979) 2307-2314.

[34] T.T. Basiev, E.V. Kharikov, V.I. Zhekov, T.M. Murina, V.V. Osiko, A.M. Prokhorov, M.I. Timoschechkin, I.A. Shcherbakov, Radiative and Non-radiative

transitions exhibited by Er^{3+} ions in mixed yttrium-erbium Aluminum garnets, Sov. J. Quantum. Electron. 6 (1976) 796-799.

[35] F. Priolo, G. Franzò, S. Coffa, A. Carnera, Excitation and nonradiative deexcitation processes of Er^{3+} in crystalline Si, Phys. Rev. B 57 (1998) 4443-4455.

[36] D.M. Henry, J.H. Herringer, N. Djeu, Response of the 1.6 μm Er:$Y_3Al_5O_{12}$ fiber-optic temperatures sensor up to 1520K, Appl. Phys. Lett. 74 (1999) 3447-3449.

[37] M.K. Ashurov, T.T. Basiev, Y.K. Voron´ko, E.V. Zharikov, V.I. Zhekov, T.M. Murina, V.V. Osiko, M.I. Timoshechkin, I. A. Shcherbakov, Nonradiative losses due to the $^4I_{11/2}$-$^4I_{13/2}$ transitions of the Er^{3+} ion in $Y_3Al_5O_{12}$, $Gd_3Sc_2Al_3O_{12}$, $Y_3Ga_5O_{12}$, $Gd_3Ga_5O_{12}$ and CaF_2 crystals, Sov. J. Quantum Electron. 8 (1978) 588-591.

[38] N. Yamada, S. Shionoya and T. Kushida. Phonon-Assisted Energy Transfer between Trivalent Rare Earth Ions, J. Phys. Soc. Jpn. 32 (1972) 1577-1586.

Figure captions

Figure 1: SEM micrographs showing the microstructure of the transverse cross-section of the AE003 and AE03 eutectic samples solidified at 25 mm/h and 750 mm/h. x in the upper row indicates the erbium concentration in the garnet phase ($Er_xY_{3-x}Al_xO_{12}$) for the corresponding column.

Figure 2: Attenuation coefficient at room temperature of the in-line transmission of the eutectics Al_2O_3-$Y_{3-x}Er_xAl_5O_{12}$ solidified at 750 mm/h and measured on transverse polished slices 140 to 150 μm thick. Solid line (x=3), dot-dashed line (x=0.3) and dashed line (x=0.03).

Figure 3: $^4S_{3/2}$ to $^4I_{15/2}$ luminescence spectra at room temperature of the eutectics Al_2O_3-$Y_{3-x}Er_xAl_5O_{12}$ grown at 25 mm/h and of the garnet single crystal EAG, excited at 514.5 nm by an argon laser. Red line (x=3), green line (x=0.3), blue line (x=0.03) and dotted black line (EAG). The upper spectrum shows the luminescence spectrum of the AE03 sample excited at 488 nm with the lamp.

Figure 4: Energy level scheme of Er^{3+} in a crystal field of D_2 symmetry. The measured splittings of the $^4S_{3/2}$ and $^4I_{15/2}$ multiplets for AE003, AE03 and AE3 samples are listed in the right hand side of the figure, from left to right respectively.

Figure 5: Thermal emission spectra of the AE0, AE003, AE03 and AE3 eutectic rods grown at 750 mm/h measured at 1200ºC. For comparison purposes, the emission band centred at 1540 nm is presented in the inset, normalized to the maximum intensity.

Figure 6: Integrated area of the selective emission bands (background subtracted) at 1540 nm (solid circles) and 970 nm (open circles) measured at 1200ºC as a function of the erbium content for the AE3, AE03 and AE003 rods grown at 750 mm/h. The

intensity of the band centred at 970 nm is amplified by a factor of 5. Dashed lines are just an eye guide. For comparison purposes, solid lines show the selective emission increase proportional to the erbium content.

Figure 7: Calculated emissivity of 1mm thick slices of hypothetically non-scattering AE3 (solid line), AE03 (dot-dashed line) and AE003 (dashed line) composites. See text for details.

Figure 8: Thermal emission spectra of AE3 eutectic rods grown at 25 mm/h measured at 1200ºC for two samples with diameters of 1.4 mm and 0.3 mm. Spectra of both samples are presented normalized to the maximum intensity, for comparison purposes.

Figure 9: Thermal emission spectra of (a) AE03 and (b) AE3 eutectic rods grown at 25 mm/h (dotted line) and 750 mm/h (solid line) at several temperatures.

Figure 10: Integrated areas of the selective emission bands at (a) 970 nm and (b) 1540 nm for the AE3, AE03 and AE003 rods grown at 25 mm/h (solid circles) and 750 mm/h (open circles) as a function of the temperature. Solid lines represent the erbium emission calculated by using the equations given in the text and the parameters given in Table 2. Inset: Off-band emission intensity for AE3 at (a) 1200 nm and (b) 1900 nm. For comparison, the normalised blackbody emissions at the corresponding wavelengths are also given (dashed lines).

Table 1: Composition, Er^{3+} concentration, volume fractions of eutectic phases and eutectic interspacing in processed samples, λ.

sample	Starting composition	Er^{3+} ions. cm^{-3}	Eutectic volume fractions	λ (μm)
EAG	62.5% mol Al_2O_3 37.5% mol Er_2O_3	$1.41 \cdot 10^{22}$	100% EAG	
AE0	81.5% mol Al_2O_3 18.5% mol Y_2O_3	0	25 mm/h 39.9±0.7% Al_2O_3	5.1 ± 0.1
			750 mm/h 45.6 ± 1.3 % Al_2O_3	1.1 ± 0.01
AE003	81.5% mol Al_2O_3 18.31% mol Y_2O_3 0.19% mol Er_2O_3	$7.56 \cdot 10^{19}$	25 mm/h 44.2±1.5 % Al_2O_3	5.7 ± 0.5
			750 mm/h 43.5 ± 2 % Al_2O_3	0.9 ± 0.05
AE03	81.5% mol Al_2O_3 16.65% mol Y_2O_3 1.85% mol Er_2O_3	$7.56 \cdot 10^{20}$	25 mm/h 41.1±3.3 % Al_2O_3	5.7 ± 0.5
			750 mm/h 43.1 ± 2.2 % Al_2O_3	0.8 ± 0.09
AE3	81% mol Al_2O_3 19% mol Er_2O_3	$7.56 \cdot 10^{21}$	25 mm/h 41.3±0.4% Al_2O_3	6 ± 0.3
			750 mm/h 42.5±0.8% Al_2O_3	0.8 ± 0.06

Table 2: Parameter values used to simulate in figure 10 the erbium selective emission of samples grown at 25 mm/h, where $\hbar\omega_{MP}$ is the phonon energy for the multiphonon processes; W^0_{ij}, the non radiative rate at T= 0 K; $\hbar\omega_{ET}$, the phonon energy for the energy transfer processes; W_{ET}, the energy transfer rate at T= 0 K, and E_a, the activation energy for the energy transfer process. All energies are given in cm^{-1} and all rates in s^{-1}.

x	$\hbar\omega_{MP}$	W^0_{12}	W^0_{23}	W^0_{13}	$\hbar\omega_{ET}$	W_{ET} ($^4I_{13/2}$)	E_a ($^4I_{13/2}$)	W_{ET} ($^4I_{11/2}$)	E_a ($^4I_{11/2}$)
0.03	445	$6\cdot10^{-5}$	16	$<10^{-11}$	180	$7.5\cdot10^{-10}$	2910	----	2860
0.3	500	8.9	$7.3\cdot10^{3}$	$3\cdot10^{-4}$	180	$1.7\cdot10^{-6}$	2910	$3\cdot10^{-6}$	2860
3	500	8.9	$7.3\cdot10^{3}$	$3\cdot10^{-4}$	180	$3.8\cdot10^{-6}$	2910	$7\cdot10^{-6}$	2860

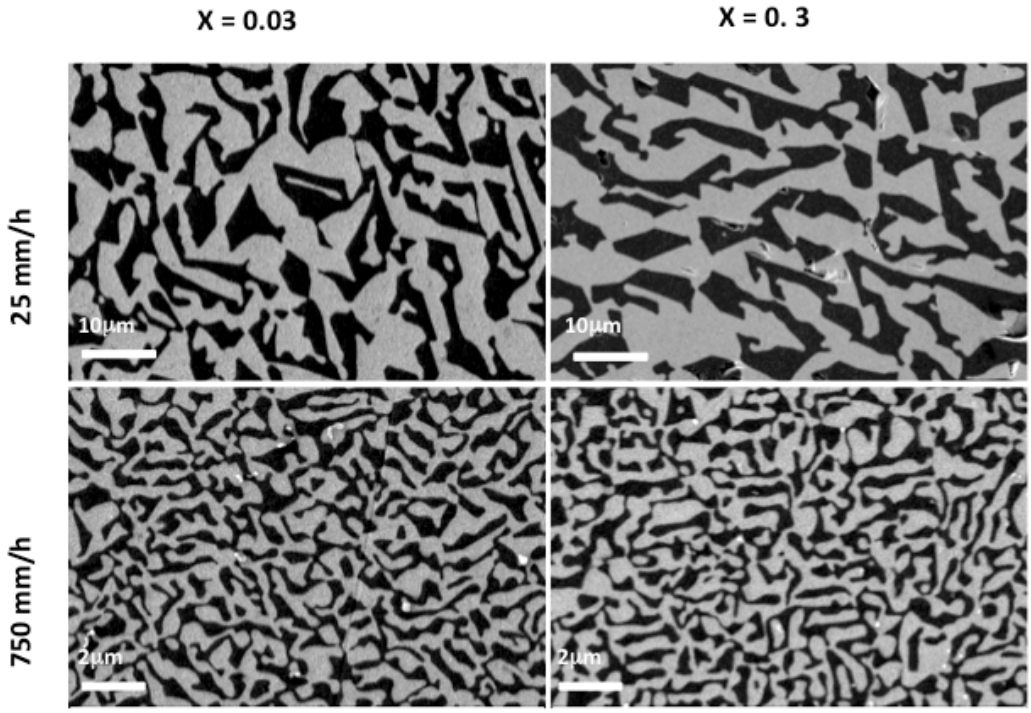

Figure 1: SEM micrographs showing the microstructure of the transverse cross-section of the AE003 and AE03 eutectic samples solidified at 25 mm/h and 750 mm/h. x in the upper row indicates the erbium concentration in the garnet phase ($Er_xY_{3-x}Al_xO_{12}$) for the corresponding column.

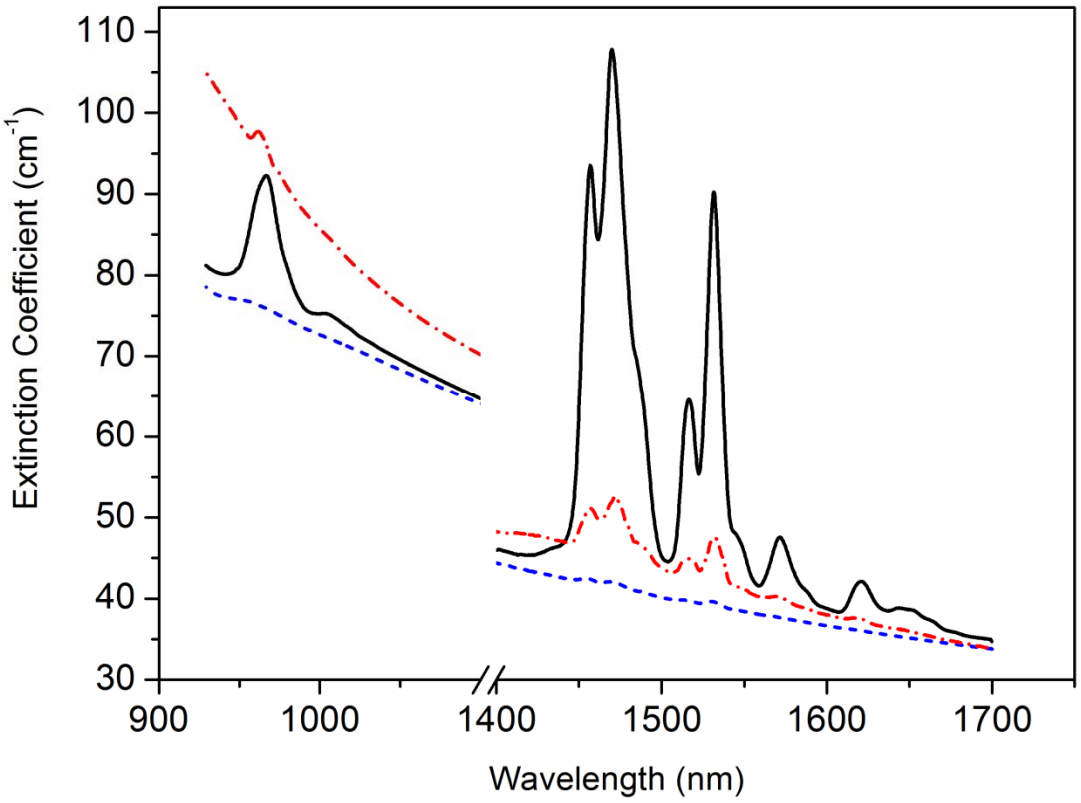

Figure 2: Attenuation coefficient at room temperature of the in-line transmission of the eutectics Al_2O_3-$Y_{3-x}Er_xAl_5O_{12}$ solidified at 750 mm/h and measured on transverse polished slices 140 to 150 µm thick. Solid line (x=3), dot-dashed line (x=0.3) and dashed line (x=0.03).

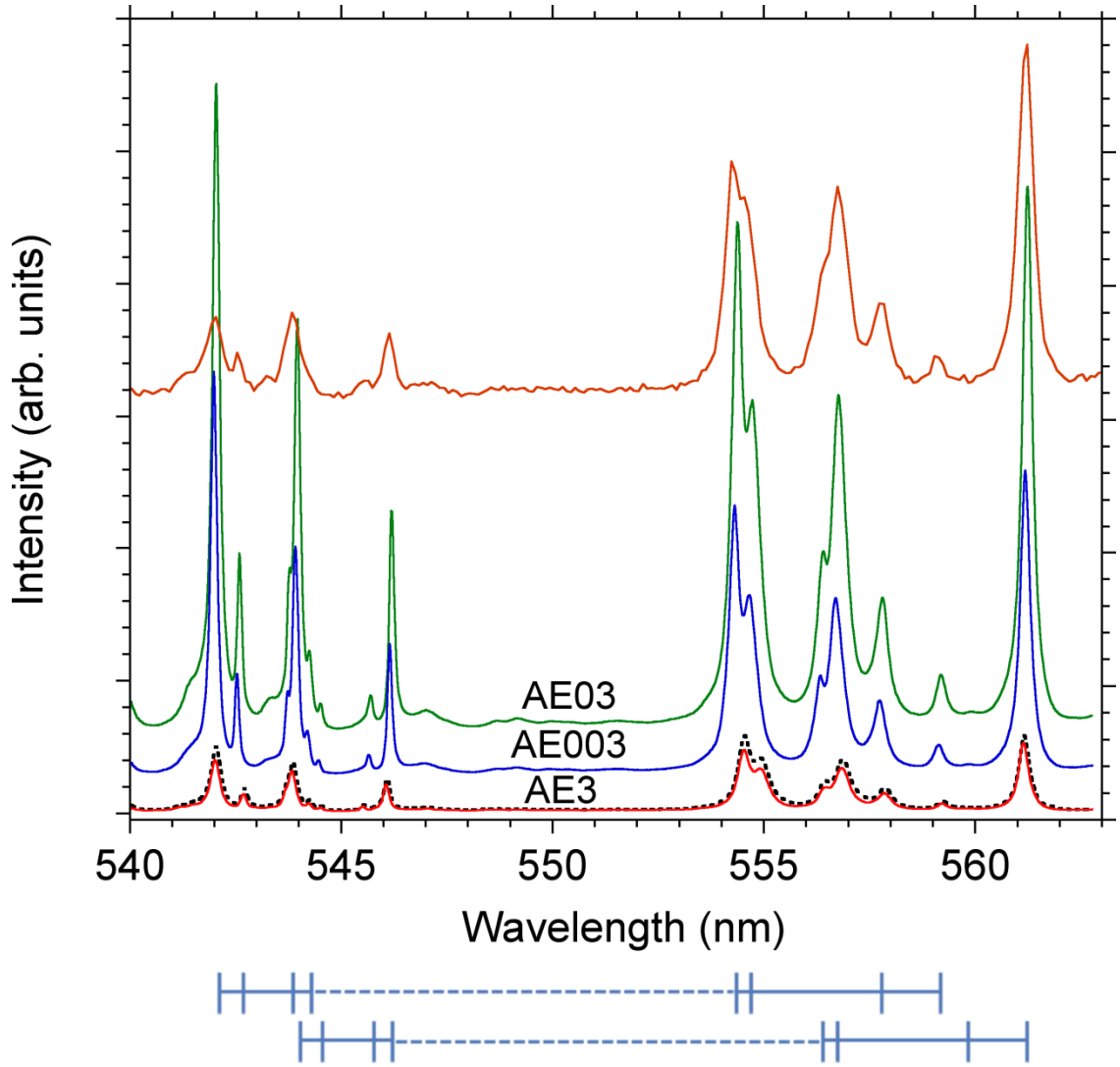

Figure 3: $^4S_{3/2}$ to $^4I_{15/2}$ luminescence spectra at room temperature of the eutectics Al_2O_3-$Y_{3-x}Er_xAl_5O_{12}$ grown at 25 mm/h and of the garnet single crystal EAG, excited at 514.5 nm by an argon laser. Red line (x=3), green line (x=0.3), blue line (x=0.03) and dotted black line (EAG). The upper spectrum shows the luminescence spectrum of the AE03 sample excited at 488 nm with the lamp.

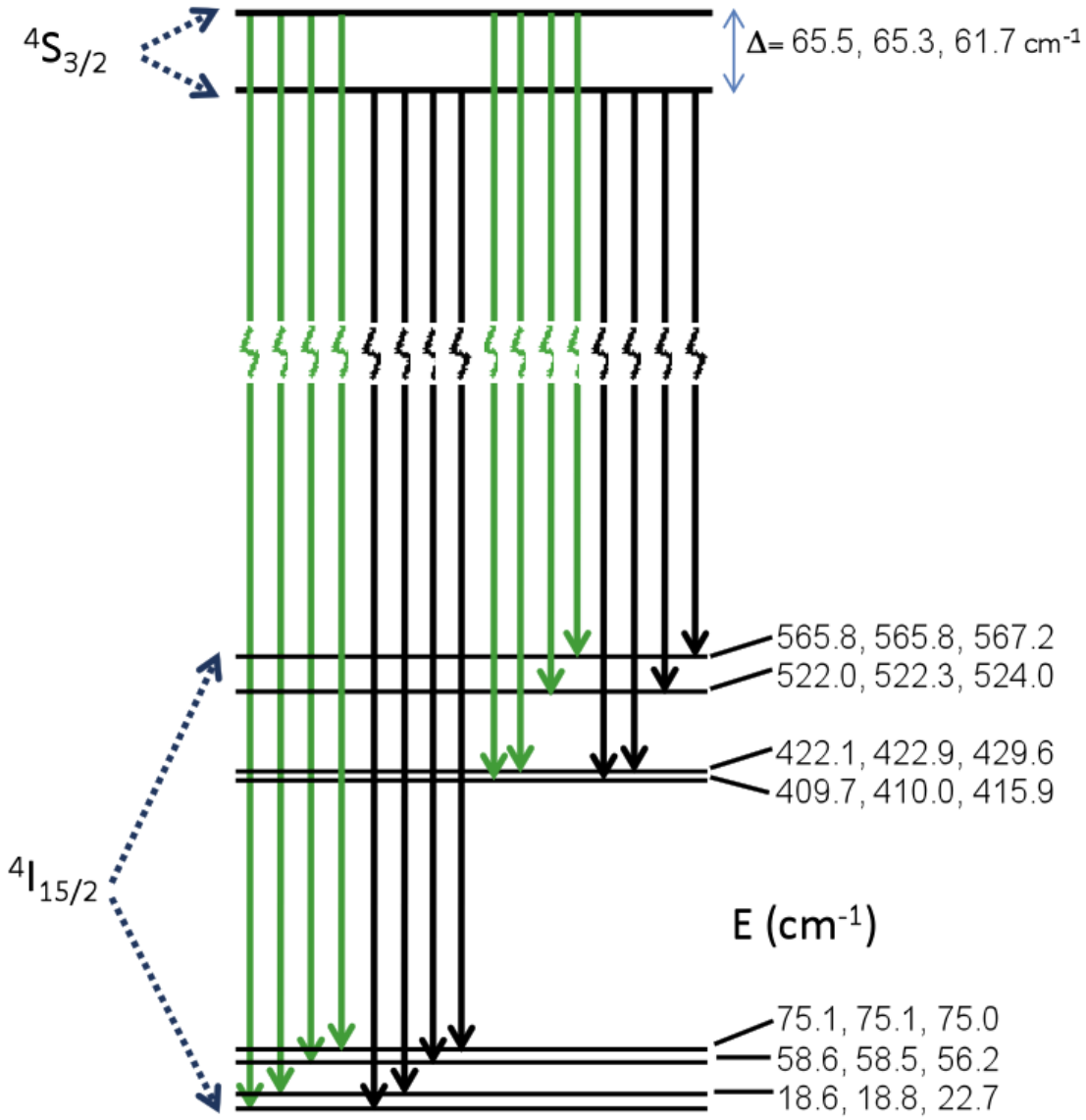

Figure 4: Energy level scheme of Er^{3+} in a crystal field of D_2 symmetry. The measured splittings of the $^4S_{3/2}$ and $^4I_{15/2}$ multiplets for AE003, AE03 and AE3 samples are listed in the right hand side of the figure, from left to right respectively.

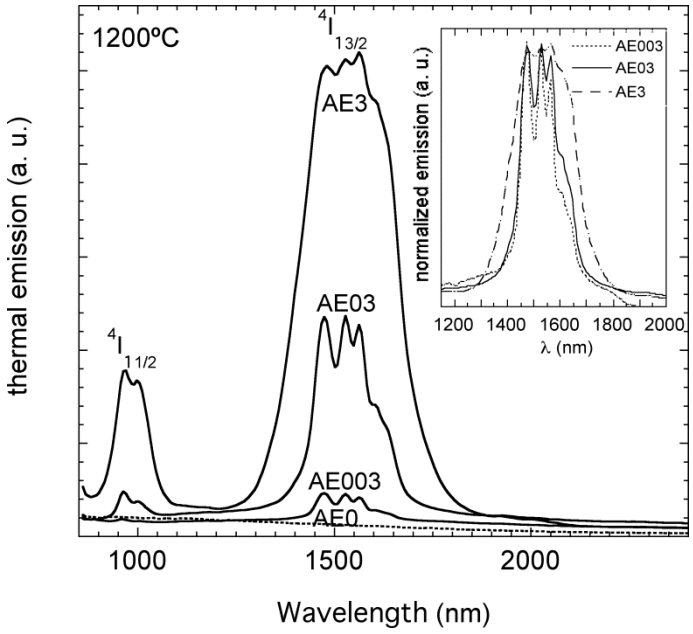

Figure 5: Thermal emission spectra of the AE0, AE003, AE03 and AE3 eutectic rods grown at 750 mm/h measured at 1200ºC. For comparison purposes, the emission band centred at 1540 nm is presented in the inset, normalized to the maximum intensity.

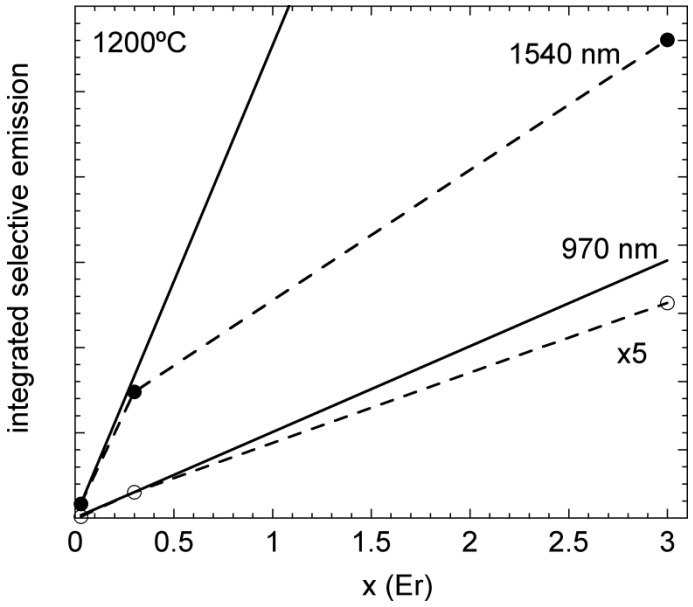

Figure 6: Integrated area of the selective emission bands (background subtracted) at 1540 nm (solid circles) and 970 nm (open circles) measured at 1200ºC as a function of the erbium content for the AE3, AE03 and AE003 rods grown at 750 mm/h. The intensity of the band centred at 970 nm is amplified by a factor of 5. Dashed lines are just an eye guide. For comparison purposes, solid lines show the selective emission increase proportional to the erbium content.

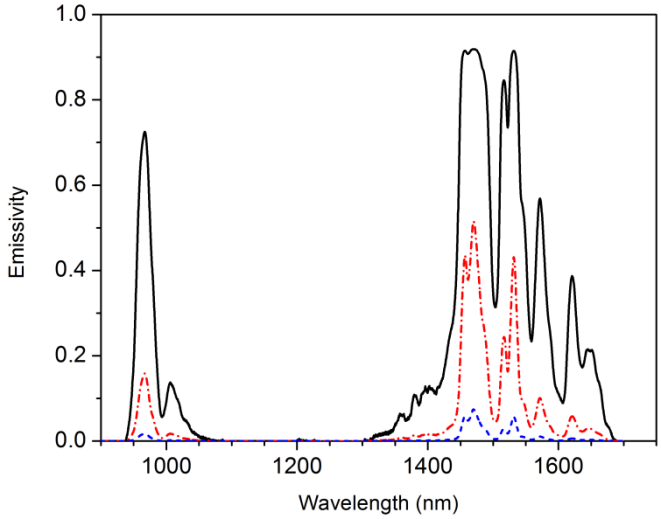

Figure 7: Calculated emissivity of 1mm thick slices of hypothetically non-scattering AE3 (solid line), AE03 (dot-dashed line) and AE003 (dashed line) composites. See text for details.

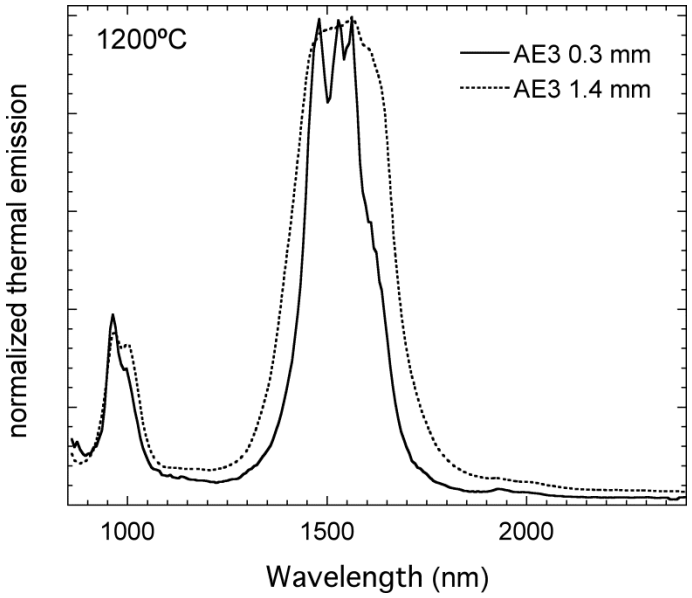

Figure 8: Thermal emission spectra of AE3 eutectic rods grown at 25 mm/h measured at 1200ºC for two samples with diameters of 1.4 mm and 0.3 mm. Spectra of both samples are presented normalized to the maximum intensity, for comparison purposes.

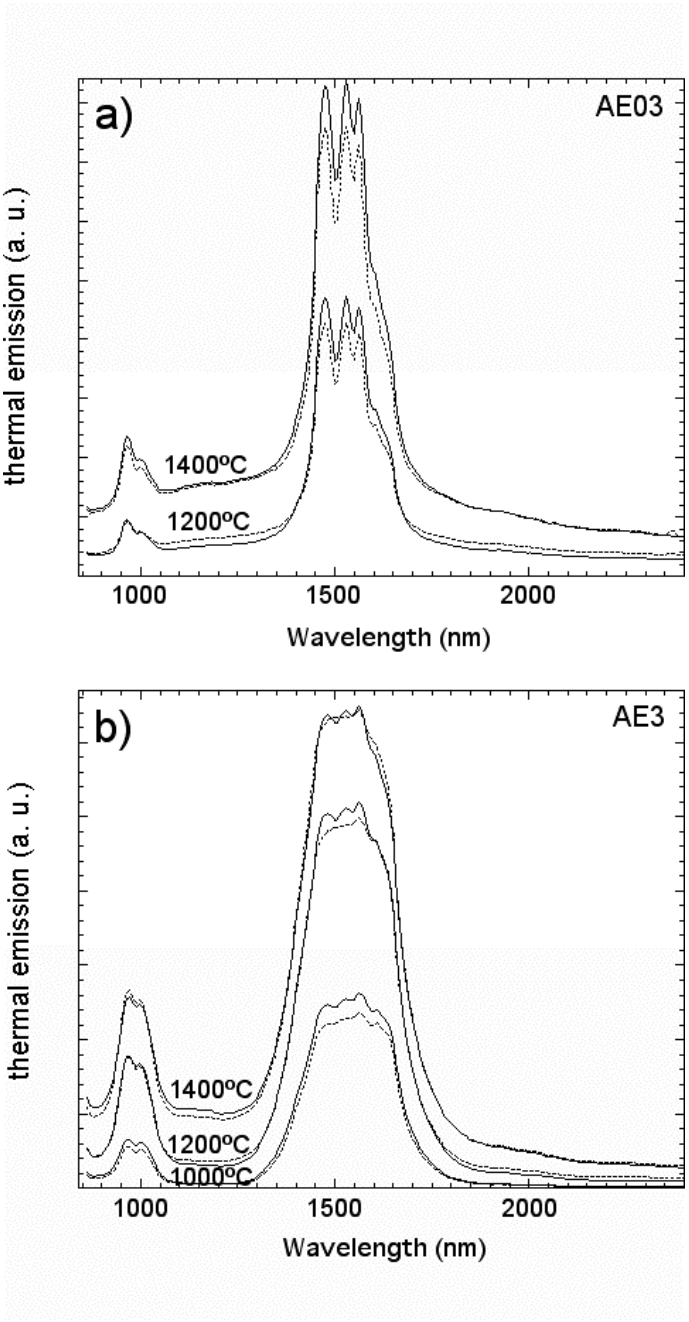

Figure 9: Thermal emission spectra of (a) AE03 and (b) AE3 eutectic rods grown at 25 mm/h (dotted line) and 750 mm/h (solid line) at several temperatures.

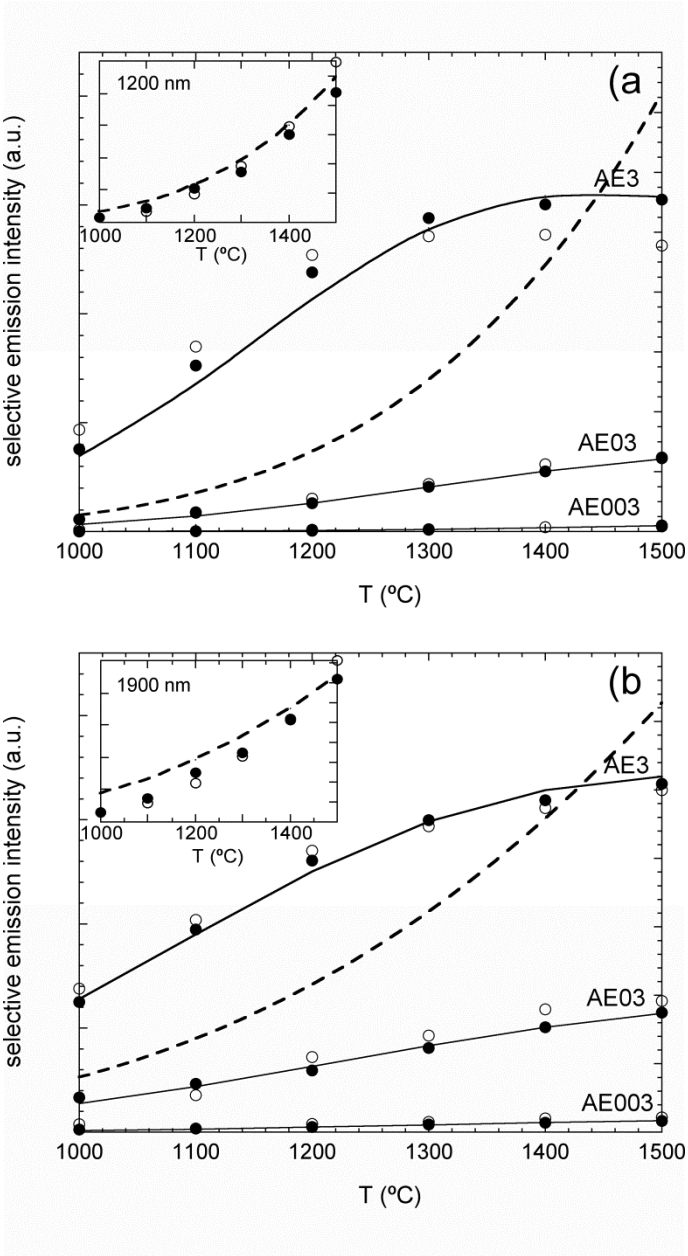

Figure 10: Integrated areas of the selective emission bands at (a) 970 nm and (b) 1540 nm for the AE3, AE03 and AE003 rods grown at 25 mm/h (solid circles) and 750 mm/h (open circles) as a function of the temperature. Solid lines represent the erbium emission calculated by using the equations given in the text and the parameters given in Table 2. Inset: Off-band emission intensity for AE3 at (a) 1200 nm and (b) 1900 nm. For comparison, the normalised blackbody emissions at the corresponding wavelengths are also given (dashed lines).